Langmuir
Article

pubs.acs.org/Langmuir

Pt_3Te_4 Nanoparticles from Tellurium Nanowires

A. K. Samal and T. Pradeep*

DST Unit on Nanoscience (DST UNS), Department of Chemistry, Indian Institute of Technology Madras, Chennai 600 036, India

Received August 31, 2010. Revised Manuscript Received October 21, 2010

We report the synthesis of platinum telluride nanoparticles (Pt_3Te_4 NPs) in the solution phase at room temperature using a template-assisted method. The dendrimeric aggregates formed are composed of several small units of Pt_3Te_4 NPs of ~4 nm diameter. Tellurium nanowires (Te NWs) are used as the template and the reducing agent in the growth of NPs which occurs due to the galvanic replacement reaction between Te NWs and $PtCl_6^{2-}$. Surface-enhanced Raman scattering (SERS) of the dispersed Pt_3Te_4 NPs was studied using crystal violet (CV) as the analyte. SERS sensitivity up to 10^{-8} M of CV was observed. The Raman enhancement factor (EF) of adsorbed CV on NP aggregates was calculated to be 1.74×10^5. The catalytic ability of the as-synthesized Pt_3Te_4 NPs for the reduction of 4-nitrophenol (4-NP) was studied.

Introduction

Transition metal chalcogenides have been extensively studied in view of their diverse properties. Nanocrystalline forms of these chalcogenides exhibit numerous fascinating and useful properties which are different from their bulk counterparts.[1−3] Their size-dependent optical, physical, and chemical properties have been explored. Among the transition metal chalcogenides, tellurides have been a subject of intense research due to their wide range of applications in solar cells, photovoltaics, photodetectors, thermoelectrics, optoelectronics, data storage device, biolabels, and diagnostics.[4−14] An example of such transition metal chalcogenides is platinum telluride. Nanoscale materials of the constituent elements Pt and Te have also been interesting from a number of perspectives. Platinum has been used as a catalyst and electrode in surface chemistry and electrochemistry, respectively.[15−17] Platinum catalysts are also used in fuel cells and purification of automotive exhaust gases. Apart from this, platinum has been used as a substrate for surface-enhanced Raman spectroscopy (SERS).[18−23] Widely used in conventional Raman are the roughened surfaces of coinage metals such as Au, Ag, and Cu. Te is a p-type semiconductor having a narrow band gap of 0.35 eV[24] and is an excellent candidate for photoconductivity, thermoelectricity, and piezoelectricity.[25−28] Binary nanosystems of Pt and Te, a combination of a metal and a semiconductor, are important for their potential use in the field of sensors, nanodevices, and magnetic memories.[29−31] Composites of $PtTe_2$ are known to have enhanced properties.[32,33] PbTe−$PtTe_2$ multiphase nanoparticles show enhanced Seebeck coefficient as compared to bulk PbTe.[32] Multicomponent rod shaped FePt−$PtTe_2$ exhibits high coercivity ($H_c > 500$ mT) upon annealing.[33]

Template-based synthesis is the most favorable synthetic procedure for the fabrication of one-dimensional (1D) nanostructures.[34,35] Se and Te nanowires (NWs) were used as templates for the synthesis of selenides and tellurides with similar morphologies.[36−39] Xia et al. synthesized hollow nanostructures of platinum with controllable dimensions using Se NWs and colloids as templates.[40] Hollow nanostructures of platinum were obtained by

---

*To whom correspondence should be addressed. E-mail: pradeep@iitm.ac.in. Fax: 91-44-2257-0545/0509.

(1) Huang, Y.; Duan, X.; Cui, Y.; Lauhon, L. J.; Kim, K. H.; Lieber, C. M. *Science* **2001**, *294*, 1313.

(2) Xia, Y.; Yang, P.; Sun, Y.; Wu, Y.; Mayers, B.; Gates, B.; Yin, Y.; Kim, F.; Yan, H. *Adv. Mater.* **2003**, *15*, 353.

(3) Murray, C. B.; Kagan, C. R.; Bawendi, M. G. *Science* **1995**, *270*, 1335.

(4) Gunes, S.; Neugebauer, H.; Sariciftci, N. S.; Roither, J.; Kovalenko, M.; Pillwein, G.; Heiss, W. *Adv. Funct. Mater.* **2006**, *16*, 1095.

(5) Li, Y. C.; Zhong, H. Z.; Li, R.; Zhou, Y.; Yang, C. H.; Li, Y. F. *Adv. Funct. Mater.* **2006**, *16*, 1705.

(6) Zhong, H.; Zhou, Y.; Yang, Y.; Yang, C.; Li, Y. *J. Phys. Chem. C* **2007**, *111*, 6538.

(7) Norton, P. *Opto-Electron. Rev.* **2002**, *10*, 159.

(8) Venkatasubramanian, R.; Siivola, E.; Colpitts, T.; O'Quinn, B. *Nature* **2001**, *413*, 597.

(9) Yan, Q.; Chen, H.; Zhou, W.; Hng, H. H.; Boey, F. Y. C.; Ma, J. *Chem. Mater.* **2008**, *20*, 6298.

(10) Mingo, N. *Appl. Phys. Lett.* **2004**, *85*, 5986.

(11) Gaponik, N. P.; Talapin, D. V.; Rogach, A. L.; Eychmuller, A. *J. Mater. Chem.* **2000**, *10*, 2163.

(12) Batabyal, S. K.; Vittal, J. J. *Chem. Mater.* **2008**, *20*, 5845.

(13) Wang, S.; Mamedova, N.; Kotov, N. A.; Chen, W.; Studer, J. *Nano Lett.* **2002**, *2*, 817.

(14) Mamedova, N. N.; Kotov, N. A.; Rogach, A. L.; Studer, J. *Nano Lett.* **2001**, *1*, 281.

(15) Feldheim, D. L. *Science* **2007**, *316*, 699.

(16) Childers, C. L.; Huang, H.; Korzeniewski, C. *Langmuir* **1998**, *15*, 786.

(17) Chen, A.; Holt-Hindle, P. *Chem. Rev.* **2010**, *110*, 3767.

(18) Tian, Z. Q.; Yang, Z. L.; Ren, B.; Li, J. F.; Zhang, Y.; Lin, X. F.; Hu, J. W.; Wu, D. Y. *Faraday Discuss.* **2006**, *132*, 159.

(19) Tian, Z. Q.; Ren, B.; Wu, D. Y. *J. Phys. Chem. B* **2002**, *106*, 9463.

(20) Mrozek, M. F.; Xie, Y.; Weaver, M. J. *Anal. Chem.* **2001**, *73*, 5953.

(21) Leung, L. W. H.; Weaver, M. J. *Langmuir* **1988**, *4*, 1076.

(22) Roberto, G.; Jose, S. G.; Juan, M. P.; Antonio, A. *J. Raman Spectrosc.* **2005**, *36*, 613.

(23) Gomez, R.; Perez, J. M.; Gullon, J. S.; Montiel, V.; Aldaz, A. *J. Phys. Chem. B* **2004**, *108*, 9943.

(24) Song, J. M.; Lin, Y. Z.; Zhan, Y. J.; Tian, Y. C.; Liu, G.; Yu, S. H. *Cryst. Growth Des.* **2008**, *8*, 1902.

(25) Mayers, B.; Xia, Y. *J. Mater. Chem.* **2002**, *12*, 1875.

(26) Mohanty, P.; Kang, T.; Kim, B.; Park, J. *J. Phys. Chem. B* **2006**, *110*, 791.

(27) Zhang, B.; Hou, W.; Ye, X.; Fu, S.; Xie, Y. *Adv. Funct. Mater.* **2007**, *17*, 486.

(28) Weihong, X.; Jiming, S.; Lian, S.; Jinlong, Y.; Wenping, H.; Zhuoyu, J.; Hong, Y. S. *Small* **2008**, *4*, 888.

(29) Cobden, D. H. *Nature* **2001**, *409*, 32.

(30) Cui, Y.; Wei, Q.; Park, H.; Lieber, C. M. *Science* **2001**, *293*, 1289.

(31) Prinz, G. A. *Science* **1998**, *282*, 1660.

(32) Zhou, W.; Zhu, J.; Li, D.; Hng, H. H.; Boey, F. Y. C.; Ma, J.; Zhang, H.; Yan, Q. *Adv. Mater.* **2009**, *21*, 3196.

(33) Yan, Q.; Raghuveer, M. S.; Li, H.; Singh, B.; Kim, T.; Shima, M.; Bose, A.; Ramanath, G. *Adv. Mater.* **2007**, *19*, 4358.

(34) Martin, C. R. *Science* **1994**, *266*, 1961.

(35) Goldberger, J.; He, R.; Zhang, Y.; Lee, S.; Yan, H.; Choi, H. J.; Yang, P. *Nature* **2003**, *422*, 599.

(36) Jiang, X.; Mayers, B.; Herricks, T.; Xia, Y. *Adv. Mater.* **2003**, *15*, 1740.

(37) Tai, G.; Zhou, B.; Guo, W. *J. Phys. Chem. C* **2008**, *112*, 11314.

(38) Samal, A. K.; Pradeep, T. *J. Phys. Chem. C* **2009**, *113*, 13539.

(39) Liang, H. W.; Liu, S.; Wu, Q. S.; Yu, S. H. *Inorg. Chem.* **2009**, *48*, 4927.

(40) Mayers, B.; Jiang, X.; Sunderland, D.; Cattle, B.; Xia, Y. *J. Am. Chem. Soc.* **2003**, *125*, 13364.

the galvanic reduction of platinum salts by Se NWs. Xie et al. also synthesized Pt−Te nanochains using Te NWs as the template.[27] The formation of Pt−Te nanochains was due to the galvanic replacement reaction between Te NWs and the platinum salt. Liang et al. synthesized ultrathin Pt/Pd NWs and nanotubes with a large aspect ratio of ~10 000 using ultrathin Te NWs as both the reducing agent and the sacrificial template.[41] Recently, Chang et al. synthesized different nanostructures of platinum such as nanosponges, nanonetworks, and nanodendrites by the galvanic replacement of Te NWs and Pt^{4+}.[42] The formation of these structures was controlled via temperature and concentration of sodium dodecyl sulfate (SDS). Wang et al. synthesized Te/Pt hybrid NWs in which the growth of Pt nanoparticles (NPs) was performed on the surface of Te NWs.[43] Yu et al. discussed the synthesis of 1D nanostructures using template-directed approaches and emphasized their fabrication by templating against similar pre-existing structures.[44]

In this report, we present the galvanic replacement reaction between Te NWs and $PtCl_6^{2-}$ resulting in Pt_3Te_4 NP aggregates in aqueous phase at room temperature. SDS or any external agents are not added in the synthesis of NP aggregates. Various microscopic and spectroscopic tools were used to characterize the formed materials. SERS of the synthesized NP aggregates was studied using crystal violet (CV) as the analyte. The catalytic ability of Pt_3Te_4 NPs was studied for the transformation of 4-nitrophenol (4-NP) to 4-aminophenol (4-AP). This is the first report of the synthesis of Pt_3Te_4 in the nanoscale, enabling further studies and applications.

Experimental Section

Sodium dodecyl sulfate ($C_{12}H_{25}O_4SNa$, 99%) was obtained from Acros. Tellurium dioxide (TeO_2, 99.9%) powder was purchased from Alfa Aesar. $H_2PtCl_6 \cdot 6H_2O$ and hydrazine monohydrate ($N_2H_4 \cdot H_2O$, 99−100%) were purchased from SD Fine Chemicals, India. CV was purchased from CDH, India. Sodium borohydride ($NaBH_4$, 98%) and 4-nitrophenol ($C_6H_4OHNO_2$, 97%) were purchased from Sigma Aldrich and Libo, respectively. Deionized water was used throughout the experiment.

Synthesis of Pt_3Te_4 NPs was carried out in two steps: (1) synthesis of Te NWs and (2) reaction between Te NWs and $PtCl_6^{2-}$. Te NWs were prepared by the wet chemical method, originally described by Chang et al.[45] In a reaction, 160 mg of TeO_2 powder was slowly added to a round-bottom flask containing 100 mL of hydrazine hydrate. The reaction was allowed to continue at room temperature under constant stirring. The powder was completely dissolved and the color of the solution changed from colorless to blue after 1 h. Blue color indicated the formation of Te NWs. After 1 h, the solution was diluted 10-fold with 10 mM SDS, in order to control the length of the NWs. The as-prepared solution was purified by centrifugation at 35 000*g* for 10 min to remove excess hydrazine and SDS. The residue was redispersed in deionized water and centrifuged twice for the complete removal of unreacted species.

For the synthesis of Pt_3Te_4 NPs, 100 mL of $PtCl_6^{2-}$ (10 mM) was added to a round-bottom flask containing 900 mL of the purified Te NWs. The ratio of molar concentrations (Te/Pt) in the solution was 1:1. The reaction mixture was stirred at room temperature. After 24 h, the color of the reaction mixture changed from blue to black. The product was centrifuged at 35 000*g* for 10 min, and the process was repeated thrice for the complete removal of unwanted species. The residue was redispersed in deionized water for further characterization. Concentrated sample was freeze-dried to make Pt_3Te_4 NP powder for further studies. Experiments were also carried out with different concentrations of $PtCl_6^{2-}$ so that the Te/Pt molar ratios were 1:3 and 3:1.

Characterization. UV−visible absorption spectra were recorded using a Perkin-Elmer Lambda 25 spectrophotometer in the range 200−1100 nm. High-resolution transmission electron microscopy (HRTEM) and energy dispersive analysis of X-rays (EDAX) were carried out with an Oxford EDAX apparatus housed in a JEOL 3010, 300 kV instrument equipped with a UHR polepiece. The samples were prepared by dropping the dispersion on carbon coated copper grids and drying in ambience. Scanning electron microscopy (SEM) and EDAX were carried out using a FEI QUANTA-200 SEM instrument, and the samples were prepared on conducting indium tin oxide (ITO) glass plates. X-ray diffraction (XRD) data were collected with a Bruker AXS, D8 Discover diffractometer using Cu Kα (λ = 1.54 Å) radiation. The samples were scanned in the 2θ range from 10 to 90°. All the peaks were assigned and compared with the database published by the Joint Committee on Powder Diffraction Standards (JCPDS). X-ray photoelectron spectroscopy (XPS) measurements were done using an Omicron ESCA Probe spectrometer with polychromatic Mg Kα X-rays ($h\nu$ = 1253.6 eV). Raman spectra were studied by using a WiTec GmbH confocal micro Raman equipped with a charge coupled device (CCD) detector. The light source was a frequency doubled Nd:YAG laser of 532 nm wavelength.

Results and Discussion

The absorption spectra of Pt_3Te_4 NPs were measured and compared with that of parent Te NWs (Figure 1A). Te NWs show two characteristic peaks: peak I and peak II. Peak I is due to the transition from p-bonding valence band (VB2) to the p-antibonding conduction band (CB1) and it appears in the range of 250−350 nm. Peak II is due to the transition from the p-lone pair valence band (VB3) to the p-antibonding conduction band (CB1) and it appears around 600−850 nm.[45−47] In this particular synthesis, peak I appeared at 279 nm and peak II appeared at 670 nm. After 6 h of the reaction with $PtCl_6^{2-}$, the absorption peaks were found to shift slightly. Peak I shifted about 2 nm from 279 to 277 nm, and peak II shifted 6 nm from 670 to 664. After 24 h, the reaction was complete with the disappearance of the peaks and only a broad peak was observed around 509 nm, signifying the formation of isotropic particles. XRD patterns of the as-prepared Te NWs and Pt_3Te_4 NPs were characterized and compared with the standard data from JCPDS (Joint Committee on Powder Diffraction Standards). All the peaks of Te NWs in the XRD pattern (Supporting Information Figure S1A) may be assigned to the hexagonal phase of Te, whose unit cell constants are a = 0.4451 nm and c = 0.5904 nm, which are consistent with the standard literature data (JCPDS: 36-1452). The XRD pattern of Pt_3Te_4 NPs is shown in Figures 1B. Peaks in the XRD pattern are indexed to the rhombohedral phase of Pt_3Te_4, consistent with the standard literature data (JCPDS: 88-2264).

The noticeable changes observed from the reactants to the products are that NWs changed their morphology to spherical particles. Figure 1C shows that, at 0 h, immediately after the addition of $PtCl_6^{2-}$, there was no transformation of nanorods to nanoparticles. At 6 h, a large number of Te NWs were observed along with fewer Pt_3Te_4 NPs. After 24 h of the reaction, nearly uniform Pt_3Te_4 NPs were formed with the complete disappearance of Te NWs (Figure 1E). Although TEM shows the presence

---

(41) Liang, H. W.; Liu, S.; Gong, J. Y.; Wang, S. B.; Wang, L.; Yu, S. H. *Adv. Mater*. **2009**, *21*, 1850.

(42) Lin, Z. H.; Lin, M. H.; Chang, H. T. *Chem.—Eur. J*. **2009**, *15*, 4656.

(43) Guo, S.; Dong, S.; Wang, E. *J. Phys. Chem. C* **2010**, *114*, 4797.

(44) Liang, H. W.; Liu, S.; Yu, S. H. *Adv. Mater*. **2010**, *22*, 3925.

(45) Lin, Z. H.; Yang, Z.; Chang, H. T. *Cryst. Growth Des*. **2008**, *8*, 351.

(46) Gautam, U. K.; Rao, C. N. R. *J. Mater. Chem*. **2004**, *14*, 2530.

(47) Sreeprasad, T. S.; Samal, A. K.; Pradeep, T. *J. Phys. Chem. C* **2009**, *113*, 1727.

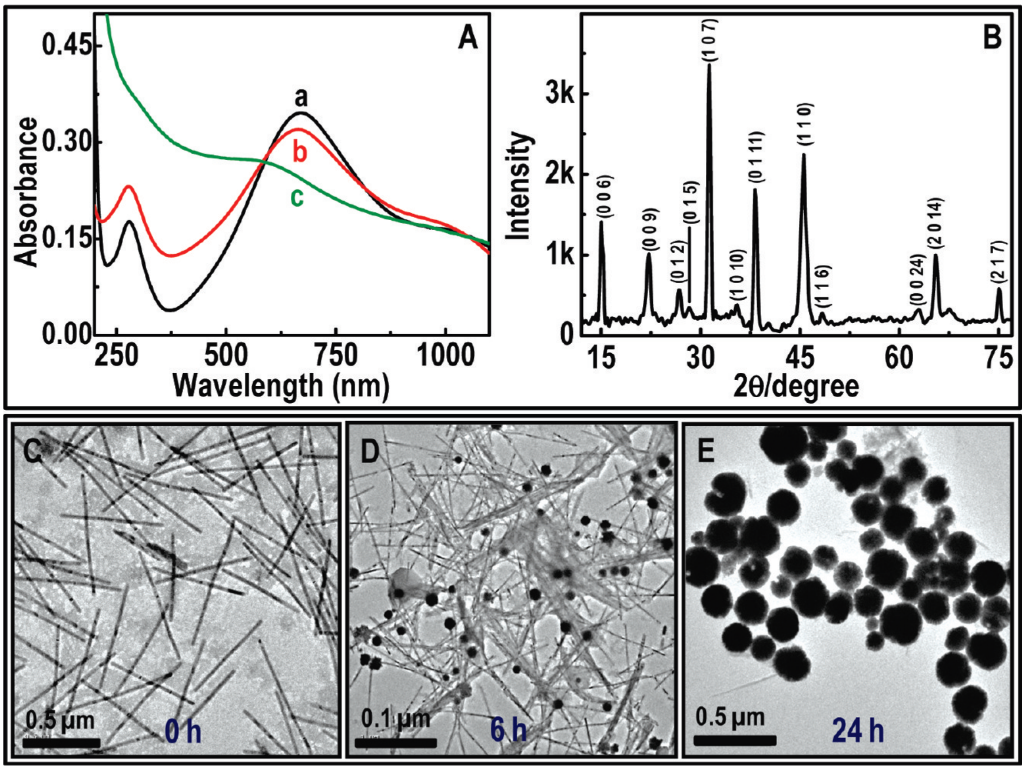

Figure 1. (A) UV−visible spectra: (a) parent Te NWs, (b) after 6 h of reaction, and (c) after 24 h of reaction. (B) XRD pattern of Pt_3Te_4. (C−E) TEM images of growth at different intervals of time.

of large particles, each of the particles is an aggregate of nanoscale particles, and therefore, we prefer to call them NPs.

TEM images of the as prepared Te NWs and Pt_3Te_4 particles have been studied. A large area TEM image of Te NWs is shown in Figure 1C. Length of the Te NWs is around 600 ± 50 nm and width is around 20 ± 4 nm. A lattice resolved HRTEM image of the body of a Te NW is shown in Figure S1B in the Supporting Information. The interplanar spacing is found to be 0.59 nm, which corresponds to the (001) plane of Te. All the NWs were straight and almost uniform in length. There were no dislocation and planar defects on the NWs, which suggest their single crystalline nature. After the addition of $PtCl_6^{2-}$, the Te NWs were reduced in dimension to form Pt_3Te_4 particles and almost all Te NWs disappeared after 24 h. Figure 2A shows the large area TEM image of Pt_3Te_4 NPs. The diameter of the Pt_3Te_4 NP aggregates was ~200 ± 30 nm. Figure 2B shows the lattice resolved HRTEM image of the edge of an aggregate showing an individual particle. It is difficult to image the center part of the NPs due to the dense packing of crystallites and consequent poor transmission. The lattice planes are resolved only at the outer edge of the NPs. Each aggregate is a collection of several smaller Pt_3Te_4 crystallites and possesses no amorphous regions. The smaller crystallites of Pt_3Te_4 NPs with average size ~4 nm are marked with circles in Figure 2B. TEM data are similar to that reported for Pt NPs which show dendrimeric growth.[48,49] The interplanar spacing of the smaller NP is 0.28 nm corresponding to the (107) plane of Pt_3Te_4.

A large area SEM image of Pt_3Te_4 NPs is shown in Figure 2C. Similar morphologies were observed in accordance with TEM. Figure 2D shows the EDAX spectrum of Pt_3Te_4 NPs, indicating the presence of Pt and Te, quantitatively. The presence of Si and Sn peaks in Figure 2D is due to the ITO conducting glass plate used as the substrate for SEM measurements.

The presence of Pt and Te in Pt_3Te_4 NPs was again confirmed by elemental analysis, via TEM-EDS. Figure 3B and C shows Te and Pt images of a single NP aggregate confirming the chemical composition at the single particle level. Figure 3A shows the corresponding TEM image of the Pt_3Te_4 NP studied. The EDAX spectrum is shown as Figure 3D. The atomic ratio of Pt to Te obtained from quantitative analysis of Pt Lα and Te Lα in the EDAX spectrum is 3:3.99, giving stoichiometric Pt_3Te_4.

In order to understand the chemical nature of the Pt_3Te_4 NPs, the sample was characterized by XPS. A survey spectrum of the sample is shown in Figure S2 in the Supporting Information. Expanded core level spectra of Pt 4f and Te 3d are shown in Figure 4. Two most intense peaks were observed at 71.2 and 74.6 eV for Pt 4f (Figure 4A), corresponding to $4f_{7/2}$ and $4f_{5/2}$, respectively. The spin−orbit splitting between Pt $4f_{7/2}$ and $4f_{5/2}$ states is 3.3 eV. These binding energies correspond to Pt(0) which are in agreement with the literature. The core level spectrum of Te 3d shows two intense peaks at 573.2 and 583.5 eV due to Te $3d_{5/2}$ and Te $3d_{3/2}$, respectively (Figure 4B). Along with the two main tellurium peaks, two weak features were observed at 577.1 and 587.7 eV, which may be assigned to Te^{4+}, due to TeO_2 of the surface. The XPS data of Te are similar to those reported previously.[50,24] The lower binding energy features may be attributed to Te(0).

Experiments were carried out at different concentrations of $PtCl_6^{2-}$ (Te NWs/$PtCl_6^{2-}$ = 1:3 and 3:1), and products were analyzed via XRD. All the peaks were assigned and compared with the standard literature values. At higher concentration of $PtCl_6^{2-}$ (Te NWs/$PtCl_6^{2-}$ = 1:3), Pt (JCPDS: 04-0802) was observed along with Pt_3Te_4 (JCPDS: 88-2264) (Supporting Information Figure S3).

---

(48) Bigall, N. C.; Hartling, T.; Klose, M.; Simon, P.; Eng, L. M.; Eychmuller, A. *Nano Lett*. **2008**, *8*, 4588.

(49) Song, Y.; Yang, Y.; Medforth, C. J.; Pereira, E.; Singh, A. K.; Xu, H.; Jiang, Y.; Brinker, C. J.; Swol, F. V.; Shelnutt, J. A. *J. Am. Chem. Soc*. **2003**, *126*, 635.

(50) Bahl, M. K.; Watson, R. L.; Irgolic, K. J. *J. Chem. Phys*. **1977**, *66*, 5526.

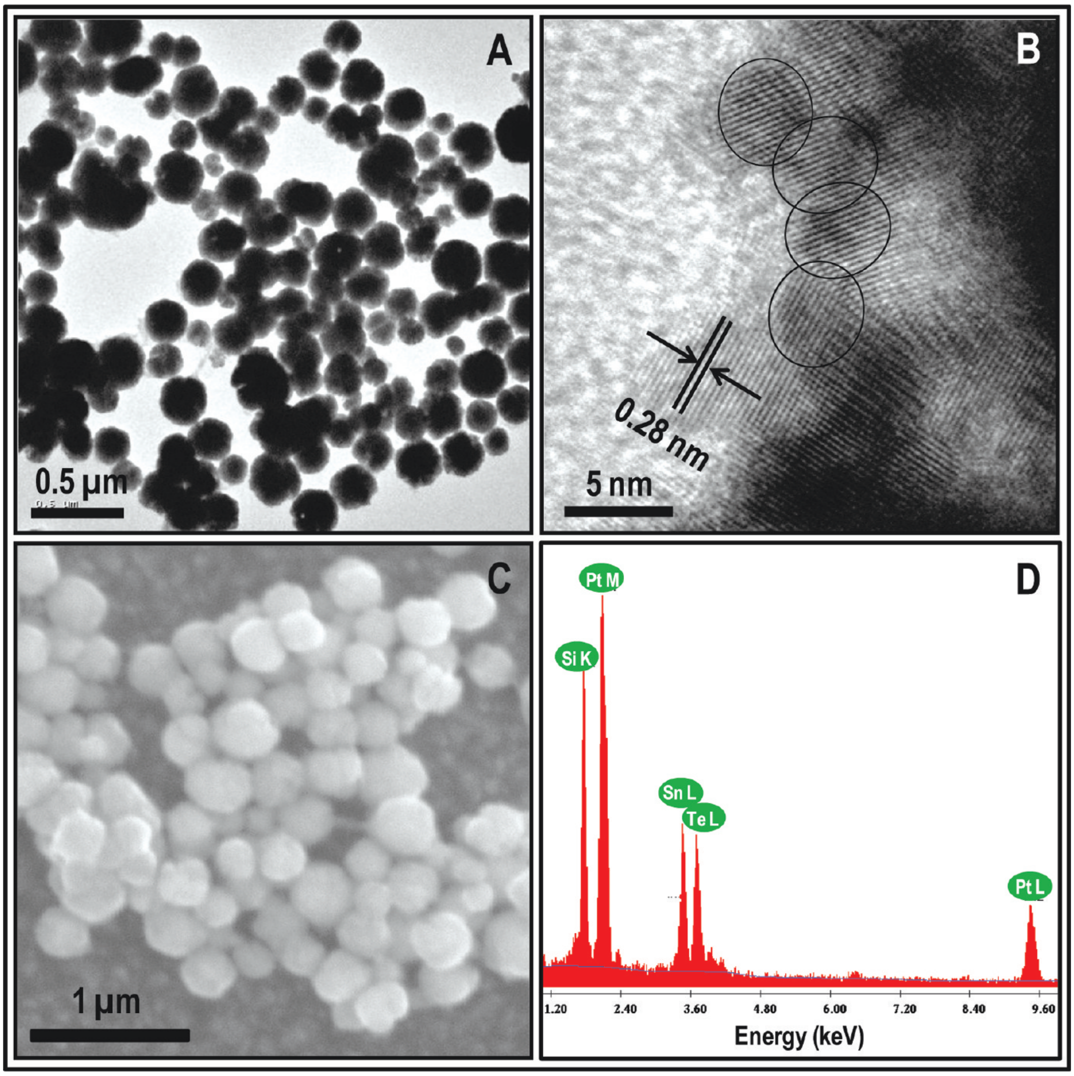

Figure 2. (A) Large area TEM image of Pt_3Te_4 NPs, (B) HRTEM image of a single Pt_3Te_4 NP aggregate, (C) large area SEM image of Pt_3Te_4 NPs, and (D) EDAX spectrum Pt_3Te_4 NPs collected using the SEM. Si and Sn peaks in D are due to the ITO conducting glass plate used as the substrate for SEM measurements.

At lower concentration of $PtCl_6^{2-}$ (Te NWs/$PtCl_6^{2-}$ = 3:1), Te (JCPDS: 36-1452) was observed along with Pt_3Te_4 (JCPDS: 88-2264) (Supporting Information Figure S4). With the available information, we propose the following mechanism for the particle growth. It is expected that the dissolution of templates and renucleation of nanocrystals happen simultaneously. Time dependent studies reveal that Te NWs started to break, forming short pieces (Supporting Information Figure S5) upon the addition of $PtCl_6^{2-}$. This may be attributed to the faster diffusion of Te out of the NW as its atomic radius is smaller than Pt. This induces vacancies in the Te NWs, causing them to rupture.[51] Smaller Te NWs reacted with $PtCl_6^{2-}$ to form smaller Pt_3Te_4 NPs, and aggregation of these smaller NPs formed bigger NPs. During the galvanic replacement between Te and $PtCl_6^{2-}$, Te NWs are oxidized to soluble TeO_3^{2-} and the Pt formed results in Pt_3Te_4 NPs.[41,52] The plausible reaction sequence may be given as follows.

$$PtCl_6^{2-} + Te + 3H_2O \rightarrow Pt + TeO_3^{2-} + 6HCl$$

$$3Pt + 4Te \rightarrow Pt_3Te_4$$

The ionic species are removed by centrifugation. Note that H_2PtCl_6 is the precursor for Pt and it is likely that acid aids in the reaction. In agreement with the mechanism, the pH of the solution decreased after the reaction.

We found that the Pt_3Te_4 phase in the only reaction product. This is explained based on the phase diagram of the Pt/Te system.[53] It is suggested that in the equal concentration range of Pt and Te, the dominant phase at all temperatures is Pt_3Te_4. All other phases exist only when one of the elements is deficient. In such cases, impurities of the excess element are also likely in the product formed. Besides this reason, Pt_3Te_4 phase is the most thermodynamically stable one than the others such as PtTe, $PtTe_2$ and Pt_2Te_3. The Pt_2Te_3 phase undergoes temperature induced transformation to Pt_3Te_4.[53]

SERS is one of the most sensitive analytical techniques which gives vibrational information when molecules are adsorbed onto metallic nanostructures.[54,55] Surface enhancement at roughened metal surfaces is very strong for coinage metals such as silver, gold, and copper. Platinum is well-known for its catalytic properties as

---

[51] Tai, G.; Guo, W.; Zhang, Z. *Cryst. Growth Des.* **2008**, *8*, 2906.
[52] Lin, Z. H.; Chang, H. T. *Langmuir* **2007**, *24*, 365.
[53] Kim, W. S. *Met. Mater.* **1996**, *2*, 9.
[54] Moskovits, M. *Rev. Mod. Phys.* **1985**, *57*, 783.
[55] Chang, R. K.; Furtak, T. E. *Surface Enhanced Raman Scattering*; Plenum Press: New York, 1982.

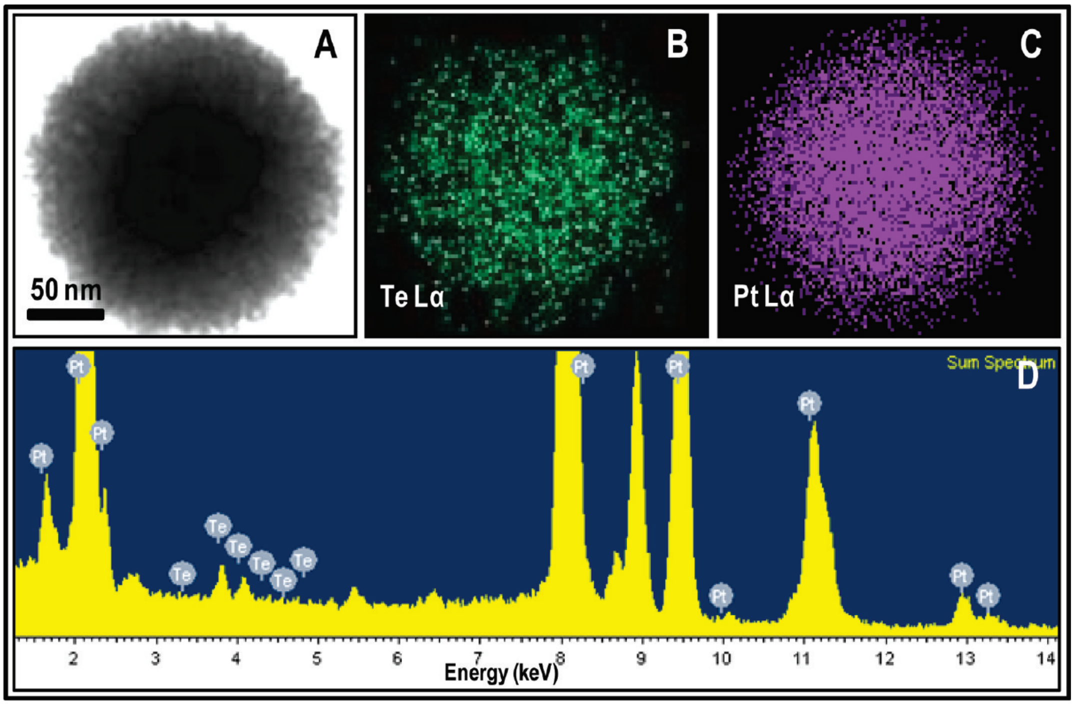

Figure 3. (A) TEM image of Pt_3Te_4 NP used for elemental mapping; (B) elemental mapping of Te and (C) Pt; and (D) EDAX spectrum of a single Pt_3Te_4 NP aggregate.

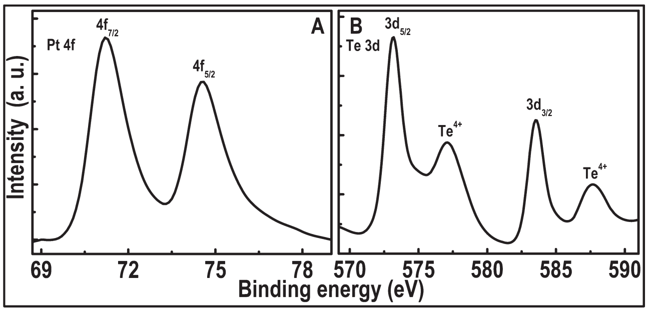

Figure 4. XPS spectra of Pt_3Te_4 NPs: (A) expanded scans of the spectrum of Pt 4f and (B) Te 3d regions. The spectrum of Te 3d shows the presence of oxides.

well as in the form of electrodes in surface chemistry and electrochemistry, and is considered as a non-SERS active metal.[16] However, different groups such as those of Tian,[18,19] Weaver,[20,21] and Perez[22,23] studied the SERS of platinum. SERS is highly morphology dependent with electromagnetic enhancement being the dominant mechanism.[56] A SERS active substrate was synthesized using Au−Te hybrid materials, and the enhancement factor (EF) of different hybrid structures was investigated.[51] We studied the SERS activity of the as prepared Pt_3Te_4 NPs using CV as the analyte molecule. The EF of adsorbed CV on NP aggregates was studied.

For the SERS measurements, the Pt_3Te_4 NP substrate was immersed in CV solution of varying concentrations for 3 h. The substrate was washed gently with distilled water and dried. Figure 5 shows the Raman spectra of CV at different concentrations exposed to Pt_3Te_4 NPs as well as to a blank glass substrate. Different concentrations of CV such as 10^{-5}, 10^{-6}, 10^{-7}, and 10^{-8} M were used. The Pt_3Te_4 NPs showed distinct Raman features of adsorbed CV even at a concentration of 10^{-8} M. At the same time, no Raman features were observed from the surface of the blank glass plate even at a higher concentration of CV (10^{-6} M). The enhancement can be explained on the basis of electric field generated at the surface upon light irradiation. Uniformly distributed Pt_3Te_4 NPs may provide efficient adsorption sites. A strong field enhancement of Pt_3Te_4 NPs may be due to the closeness of nanoparticles to each other in the aggregate, which creates the hot spots.[57,58] Local field effects may be enhanced by several orders of magnitude due to the aggregation or assemblies of nanoparticles, which show stronger SERS signals compared to isolated/individual nanoparticles. Pt_3Te_4 NPs are in close proximity to each other and form many hot spots. The plasmon coupling of Pt_3Te_4 NPs at these hot spots will produce a very strong local electromagnetic field which results in intense SERS signals.

Enhancement Factor (EF). The EF was calculated using the following relationship.[59]

$$\mathrm{EF} = (I_{\mathrm{SERS}}/I_{\mathrm{norm}})(N_{\mathrm{bulk}}/N_{\mathrm{surf}})$$

where I_{SERS}, I_{norm}, N_{bulk}, and N_{surf} are the measured SERS intensities for a monolayer of probe molecules (CV) on Pt_3Te_4 NP aggregates, the measured intensity of normal Raman scattering from a bulk sample, the number of the probe molecules under laser illumination for the bulk sample, and that on Pt_3Te_4 NP aggregates, respectively. I_{SERS} and I_{norm} are the integral intensities of the N-phenyl stretching peak at 1379 cm^{-1}. N_{surf} and N_{bulk} can be calculated using $N_{\mathrm{surf}} = 4\pi r^2 CAN$ and $N_{\mathrm{bulk}} = Ah\rho/M$, where r, C, A, and N are the average radius of the Pt_3Te_4 NPs, surface density of the CV monolayer, the area of the laser spot, and the surface coverage of Pt_3Te_4 NP aggregates, respectively. A, h, ρ, and M are the area of the laser spot, the penetration depth, the density of solid CV (~0.83 $\mathrm{g/cm^3}$), and the molecular weight of

---

(56) Hao, E.; Schatz, G. C. *J. Chem. Phys.* **2004**, *120*, 357.

(57) Lee, S. J.; Morrill, A. R.; Moskovits, M. *J. Am. Chem. Soc.* **2006**, *128*, 2200.

(58) Gunnarsson, L.; Rindzevicius, T.; Prikulis, J.; Kasemo, B.; Kall, M.; Zou, S.; Schatz, G. C. *J. Phys. Chem. B* **2005**, *109*, 1079.

(59) Shibu, E. S.; Kimura, K.; Pradeep, T. *Chem. Mater.* **2009**, *21*, 3773.

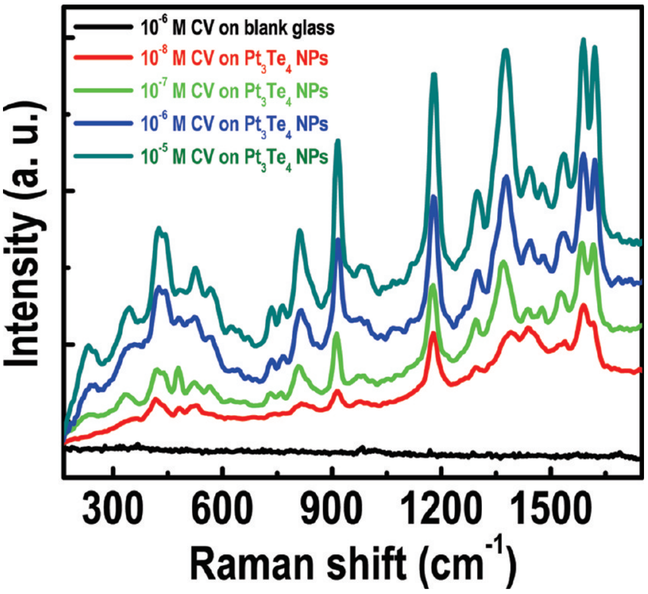

Figure 5. SERS spectra of CV at different concentrations on Pt_3Te_4 NPs.

CV, respectively. For the calculation of N_{bulk}, the sampling volume used is the product of the laser spot and the penetration depth, $\sim 2\ \mu m$. The density of CV is 0.83 g/cm^3, and $N_{\text{bulk}} = 3.2 \times 10^{-15}$ mol. The area of laser spot used was around 1 μm^2. The area required for adsorption of a CV molecule is taken to be 4 nm^2.[60] The value of EF obtained is 1.74×10^5. Although there are no SERS reports of CV on Pt nanoaggregates, we note that the calculated EF is 3 orders of magnitude higher than that of benzenethiol and three times higher than that of rhodamine 6G adsorbed on Pt nanoaggregates.[61,62]

Catalytic Reduction. Bimetallic nanoparticles of Pt were studied for their utility in catalysis. Pt−Pd clusters were used as catalysts for the hydrogenation of 1,2,3,4-tetrahydronaphtalene (tetralin).[63] Electro-oxidation of methanol in sulfuric acid solution was studied using Pt−Ni alloy.[64] Oxygen reduction reaction on carbon supports was investigated on Pt−Ni/Pt-Co alloy catalysts in aqueous acidic electrolyte at low temperature.[65] Pt−Au nanoparticles immobilized on spherical polyelectrolyte brushes were studied for the oxidation of alcohols.[66] Pal et al. studied bimetallic Pt−Ni nanoparticles for the reduction of 4-NP.[67] Here, we studied the reduction of an aromatic nitro compound, 4-NP to 4-aminophenol (4-AP), using Pt_3Te_4 NPs as the catalyst and using spectrophotometric methods.

For the catalytic reduction, 2 mL of ice cold $NaBH_4$ (100 mM) was added to 8 mL of 4-NP (1 mM). A total of 1 mg of Pt_3Te_4 NPs was added to the above solution and sonicated for the complete dispersion of Pt_3Te_4 NPs. The aqueous solution of 4-NP shows absorption features at 318 and 226 nm. Upon the addition of freshly prepared ice cold $NaBH_4$, 4-NP got converted to the phenolate ion as confirmed by the disappearance of the peak at 318 nm and appearance of a new peak at 400 nm. In the absence of the catalyst, the absorbance value and the peak position remained the same even for a couple of days. After the addition of Pt_3Te_4 NPs, the intensity of the 400 nm peak got reduced and a new peak appeared at 299 nm (Figure 6). The complete reduction of 4-NP to 4-AP occurs by 20 min, which was confirmed by the disappearance of the peak at 400 nm. The new peak at 299 nm is the characteristic absorption feature of 4-AP. The standard absorption spectrum of 4-AP is also given for comparison. The peak at 226 nm for 4-NP got shifted to 232 nm upon reduction to 4-AP. It appears that the electron donor BH_4^- provides electrons to the substrate 4-NP (acceptor) only after its adsorption on the catalyst, Pt_3Te_4. The pseudo-first-order rate constant of the disappearance of the phenolate anion, determined from the absorption spectra, is 1.3×10^{-3} s^{-1}.

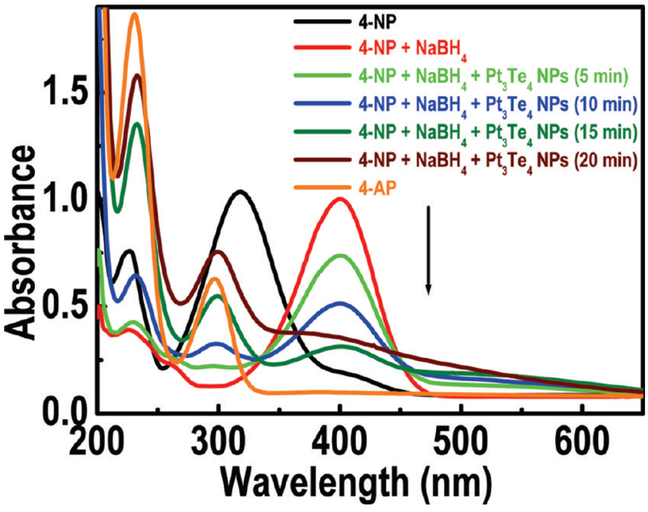

Figure 6. UV−visible spectra for the gradual reduction of 4-NP catalyzed by Pt_3Te_4 NPs.

Conclusion

Pt_3Te_4 NP aggregates were synthesized in the solution phase at room temperature using Te NWs as a reducing and sacrificial template. The NP aggregates were characterized by various microscopic and spectroscopic tools such as HRTEM, SEM, EDAX, XRD, XPS, UV−visible, and Raman. SERS of dispersed Pt_3Te_4 NPs was investigated using CV as the analyte, and a SERS sensitivity up to 10^{-8} M was observed. The EF for adsorbed CV on NP aggregates was calculated to be 1.74×10^5 which is 3 orders of magnitude higher than that measured for benzenethiol and three times more than that for rhodamine 6G adsorbed on Pt nanoaggregates. The material was used for the catalytic reduction of 4-NP. An easy method of synthesis as well as surface enhanced Raman and catalytic activities of the material are expected to generate further interest in this material.

Acknowledgment. We thank the Nano Mission of the DST, Government of India for supporting our research program on nanomaterials.

Supporting Information Available: XRD and HRTEM image of parent Te NWs. XPS survey spectrum of Pt_3Te_4 NPs. XRD of the reaction products at different concentrations of $PtCl_6^{2-}$ and TEM images of Pt_3Te_4 NPs at different time intervals during growth. This material is available free of charge via the Internet at http://pubs.acs.org.

---

(60) Kudelski, A. *Chem. Phys. Lett.* **2005**, *414*, 271.

(61) Kim, N. H.; Kim, K. *Chem. Phys. Lett.* **2004**, *393*, 478.

(62) Kim, N. H.; Kim, K. *J. Raman Spectrosc.* **2005**, *36*, 623.

(63) Rousset, J. L.; Aires, F. J. C. S.; Bornette, F.; Cattenot, M.; Pellarin, M.; Stievano, L.; Renouprez, A. J. *Appl. Surf. Sci.* **2000**, *164*, 163.

(64) Park, K. W.; Choi, J. H.; Kwon, B. K.; Lee, S. A.; Sung, Y. E.; Ha, H. Y.; Hong, S. A.; Kim, H.; Wieckowski, A. *J. Phys. Chem. B* **2002**, *106*, 1869.

(65) Paulus, U. A.; Wokaun, A.; Scherer, G. G.; Schmidt, T. J.; Stamenkovic, V.; Radmilovic, V.; Markovic, N. M.; Ross, P. N. *J. Phys. Chem. B* **2002**, *106*, 4181.

(66) Marc, S.; Sebastian, P.; Yu, M.; Rhett, K.; Nobuyoshi, M.; Matthias, B. *Adv. Mater.* **2008**, *20*, 1928.

(67) Ghosh, S. K.; Mandal, M.; Kundu, S.; Nath, S.; Pal, T. *Appl. Catal., A* **2004**, *268*, 61.